Status Report and Measurement of Total Cross-sections at the Pohang Neutron Facility

G. N. Kim,* A. K. M. M. H. Meaze, H. Ahmed, and D. Son
Institute of High Energy Physics, Kyungpook National University,
1370 Sankyuk-Dong, Puk-Gu, Daegu 702-701, Korea

Y. S. Lee, H. S. Kang, M. H. Cho, I. S. Ko, and W. Namkung
Pohang Accelerator Laboratory, Pohang University of Science and Technology,
San 31 Hyoja–Dong, Nam–Gu, Pohang 790 – 784, Korea

K. J. Yoo, Y. A. Kim and J. Chang
Korea Atomic Energy Research Institute,
150 Deokjin-dong, Yuseong-gu ,Daejeon, Korea

We report the status of the Pohang Neutron Facility which consists of an electron linear accelerator, a water-cooled Ta target, and an 11-m time-of-flight path. It has been equipped with a four-position sample changer controlled remotely by a CAMAC data acquisition system, which allows simultaneous accumulation of the neutron time of flight spectra from 4 different detectors. It can be possible to measure the neutron total cross-sections in the neutron energy range from 0.1 eV to 100 eV by using the neutron time of flight method. A ^{6}LiZnS(Ag) glass scintillator was used as a neutron detector. The neutron flight path from the water-cooled Ta target to the neutron detector was 10.81±0.02 m. The background level was determined by using notch-filters of Co, In, Ta, and Cd sheets. In order to reduce the gamma rays from Bremsstrahlung and those from neutron capture, we employed a neutron-gamma separation system based on their different pulse shapes. The present measurements are in general agreement with the evaluated data in ENDF/B-VI. The resonance parameters were extracted from the transmission data from the SAMMY fitting and compared with the previous ones.

I. INTRODUCTION

Pulsed neutrons based on an electron accelerator (linac) are a powerful tool to measure the energy dependence of cross-sections with high resolution by using time of flight (TOF). The Pohang Neutron Facility (PNF) was proposed in 1997 [1] and constructed at the Pohang Accelerator Laboratory on December 1998 [2]. It consists of a 100-MeV electron linac, water-cooled Ta neutron producing target, and an 11-m-long evacuated flight vertical tube leading to the detector location. The electron linac consists of a thermionic RF-gun, an alpha magnet, four quadrupole magnets, two SLAC-type accelerating sections, a quadrupole triplet, and a beam-analyzing magnet. A 2-m long drift space is added between the first and the second accelerating section to insert an energy compensation magnet or a beam transport magnet for other research. The overall length of the linac is about 15 m. As a photoneutron target, it is necessary to use heavy mass materials in order to produce intense neutrons by way of bremsstrahlung under high-power electron beams. We have chosen a tantalum as the target material, which has advantages of high density (16.6 g/cm^3), high melting point (3,017^{o}C), and high resistant against the corrosion by cooling water. Since we have to utilize the space and infrastructures at PAL, an 11 m long TOF path and a detector room were constructed vertically to the electron linac. The

* E-mail: gnkim@knu.ac.kr, Tel.: +82-53-950-6328

TOF tubes were made by stainless steel with two different diameters of 15 and 20 cm. The neutron beam line was equipped with a four–position sample changer which can allow the simultaneous total cross-section measurement for four different samples. The sample changer is controlled remotely by a special CAMAC module, which is part of a CAMAC data acquisition system in which great advances have resulted from simultaneous accumulation of the neutron TOF spectra from four different detectors. The facility details of PNF are described elsewhere [3].

We report the measured total cross-sections of natural Dy, Ag, Ti, and W in the neutron energy range from 0.1 eV to 100 eV by using the neutron TOF method at the PNF. The measured result was compared with the evaluated data in ENDF/B-VI. The resonance parameters for Dy and Ag were also reported and the results were compared with the previous ones.

II. EXPERIMENTAL ARRANGEMENT

The experimental arrangement for the transmission measurements is shown in Fig. 1 (a). The target is located in the position where the electron beam hits its center. To reduce the gamma-flash generated by the electron burst in the target, this one was placed 55 mm away from the center of the neutron guide. The target was composed of ten Ta plates with a diameter of 4.9 cm and an effective thickness of 7.4 cm [4]. There was a 0.15-cm water gap between Ta plates in order to cool the target effectively. The housing of the target was made of titanium. This target was set at the center of a cylindrical water moderator contained in an aluminum cylinder with a thickness of 0.5 cm, a diameter of 30 cm, and a height of 30 cm. The water level in the moderator was 3 cm above the target surface, which was decided based on a measurement of the thermal neutron flux [5]. The measurement was also compared with the Monte Carlo N-Particle (MCNP) transport code [6].

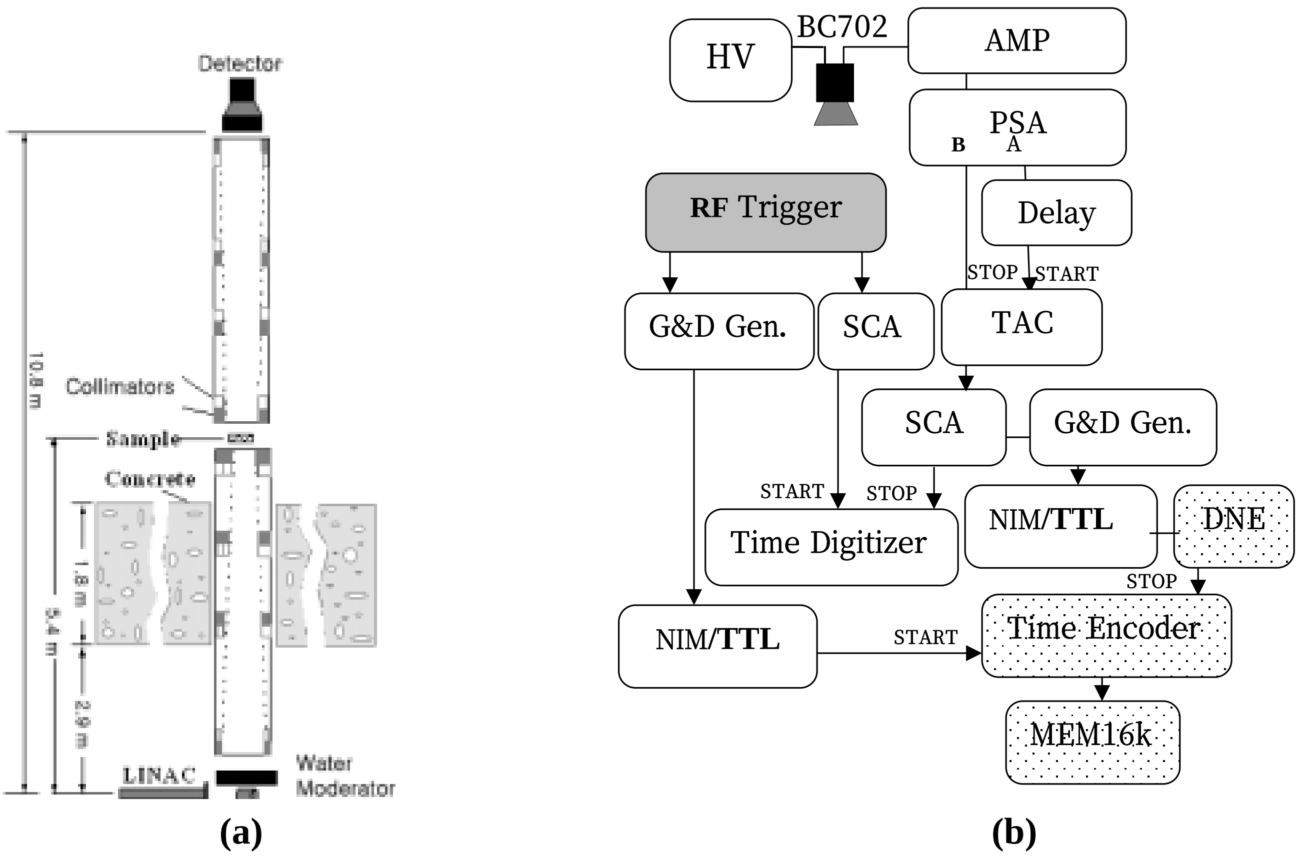

(a) (b)

Fig.1. (a) Experimental setup and (b) data acquisition system for the transmission measurements.

The neutron guide tubes were constructed of stainless steel with two different diameters, 15 cm and 20 cm, and were placed perpendicularly to the electron beam. The neutron collimation system was mainly composed of H_3BO_3, Pb and Fe collimators, which were symmetrically tapered from a 10-cm diameter at the beginning, to a 5-cm diameter in the middle position where the sample changer was located, to an 8-cm diameter at the end of guide tube where the neutron detector was placed. There was 1.8-m-thick concrete between the target and the detector room.

The sample changer consists of a disc with 4 holes; each hole is 8 cm in diameter, which matches the hole of the collimator in the neutron beam line. The sample changer, which is controlled remotely by the CAMAC module, has two important goals: Firstly, it allows data taking from up to 4 different samples simultaneously. Secondly, the exposition time for each sample may be selected individually and be precisely controlled by electronics. The last point allows systematic errors owing time variations in the neutron beam intensity to be avoided. The distance between centers of two opposite holes is 31 cm. The holders allow solid samples, as well as liquid or powder ones, to be fixed in special cassettes. The pressurized cover with a rubber O–ring prevents penetration of dust and moisture into the device. There are three windows in the sample changer: two for control and management and the other for samples downloading. All of them are transparent and pressurized. The beam transmission windows – one in the fixed disk of the sample changer, another in a top of cover (see Fig.2), are covered with aluminum foil and pressurized. The movement of the mobile disk with samples is performed by an electric motor with a built-in reduction gearbox. The time of movement between two neighboring positions is 10 sec. The mobile disk moves only in one direction, like a revolver. This decreases the backlash in fixing the sample position. Besides, a combination of an electrical and a rigid spring system allows the sample position to be fixed to better then 1 mm. Photographs of the sample changer are shown in Fig. 2.

(a) **(b)**

Fig. 2. (a) Inside part of the sample changer without a cover, and (b) outside view of the sample changer with a cover which is in its permanent location on the PNF upright neutron beam line.

The physical parameters of the samples used in the total cross-section measurements are given in Table 1. A set of notch filters of Co, Ta, and Cd plates with thickness of 0.5 mm, 0.2 mm, and 0.5 mm, respectively, was also used for the background measurement and the energy calibration. The transmission samples were placed at the midpoint of the flight path and were cycled into the neutron beam by using the automatic sample changer with four sample positions.

The neutron detector was located at a distance of 10.81 m from the photo-neutron target. A ^{6}Li-ZnS(Ag) scintillator BC702 from Bicron (Newbury, Ohio) with a diameter of 127 mm and a thickness of 15.9 mm mounted on an EMI-93090 photomultiplier was used as a detector for the neutron TOF spectrum measurement. This scintillator consists of a matrix of a lithium compound enriched to 95% ^{6}Li dispersed in a fine ZnS(Ag) phosphor powder. The detection process employs the nuclear reaction ^{6}Li (n,α)^{3}H in which the resulting α - particle and ^{3}H produce scintillations upon interacting with the ZnS(Ag).

Table 1. Physical parameters of the samples used in the experiment.

Sample	Purity (%)	Size (cm^2)	Thickness (mm)	Weight (g)
Ag	99.98	10×10	0.5	53.04
Dy	99.9	10×10	0.5	37.95
W	99.98	10×10	0.2	19.30
Ti	99.9	10×10	0.5	4.50

III. DATA TAKING AND ANALYSIS

Figure 1 (b) shows the configuration of the data acquisition system used in our measurement. Two different data acquisition systems were used for the neutron TOF spectra measurements: one for the NIM-based system and the other for the CAMAC-based system. The main purpose of the NIM-based system was neutron-gamma separation and the parallel accumulation of the neutron TOF spectra if necessary.

The dynode signal from a BC702 scintillator was connected through an ORTEC-571 amplifier (AMP) to an ORTEC-552 pulse-shape analyzer (PSA) for use in neutron-gamma separation. A fast NIM signal from the “A” output of the PSA was delayed by 60 ns and used as the start signal for an ORTEC-567 time-to-amplitude converter (TAC). The “B” output signal from the PSA was used as the stop signal for the TAC. One of TAC outputs was connected to an ORTEC-550A single channel analyzer (SCA), and the other output signal was fed to a multi-channel pulse-height analyzer (MCA) for neutron-gamma separation. The output signal of the SCA was used as stop signals for a 150-MHz Turbo MCS (Time Digitizer) and for a time encoder of the CAMAC-based system for the neutron TOF spectra measurement. The output of the SCA was sent to an ORTEC-416A gate and delay generator (G&D Gen.) and a TTL/NIM module in order to form the proper signal for the CAMAC system. This output signal was connected to a time encoder through a detector number encoder (DNE). The DNE allowed data taking from up to 4 detectors simultaneously. The time encoder had 4096 channels and a minimal dwell time of 0.5 μs. MEM16k is a memory of 16k capacity and collected the TOF spectra during the measurement.

The 10-Hz RF trigger signal for the modulator of the electron linac was connected to a G&D Gen.; one of output signals was used as the start signal for both the time digitizer and the time encoder, and the other output was sent to the counter through a TTL/NIM converter. The remote control signal from the TTL/NIM was used as the start pulse for the time digitizer for parallel data accumulation. In distinction with the direct use of the start pulse from the RF trigger for the time digitizer, this scheme temporarily interrupts the start pulse sequence while the sample changer moves. The counter has 4 independent inputs, as well as the relevant displays for data and control signals. It is used to accumulate the monitor counts for each position of the sample changer and to control the duration of sample exposure.

The CAMAC part is controlled by PC software via an interface card and crate controller (not shown in Fig. 1 (b)). The program sets and controls the following parameters:

- the numbers and quantity of actual detectors used in the measurement;
- the actual number of TOF channels and dwell time for each detector (may be different);
- the duration of the exposition for each sample as the number of starts from the linac.

It also sets the number of full turnovers of the SC and provides a data record from the MEM16K to the relevant files for future processing. Parallel data acquisition with both the Turbo-MCS system and the

CAMAC system may be used if one desires to optimize the dwell time for different regions of the TOF spectra. For example, the CAMAC time encoder dwell time may be set to 0.5 μs to get good energy resolution in the high-energy part of the TOF spectra while the simultaneous setting for the Turbo-MSC might be 1.5 μs to approach, say, 1 meV in the low-energy region of the TOF spectra. A command file written in special script language synchronizes the CAMAC and the Turbo-MCS.

In order to adjust the neutron-gamma separation circuit used in this experiment, we used two radiation sources, ^{137}Cs and ^{252}Cf. Cesium emits gamma radiation at 662 keV, and californium emits neutrons along with gamma radiation of 100 and 160 keV. The MCA pulse-height spectra of γ rays from ^{137}Cs, neutrons and γ rays from ^{252}Cf, and noise from the neutron detector are shown in Fig. 3. We can see a shape difference between the neutron and the gamma-ray pulse-height spectra. In order to discriminate the gamma-ray and the noise contribution from the neutron TOF spectra, we set the lower-level discriminator (LLD) threshold voltage of the SCA to 1.12 V in the integral operation mode. The threshold voltage of the SCA was determined as the value at which the output signal of the SCA in the oscilloscope was almost zero when increasing the LLD value from the minimum voltage. The corresponding LLD value of 1.12 V is indicated as a line in Fig. 3 (a).

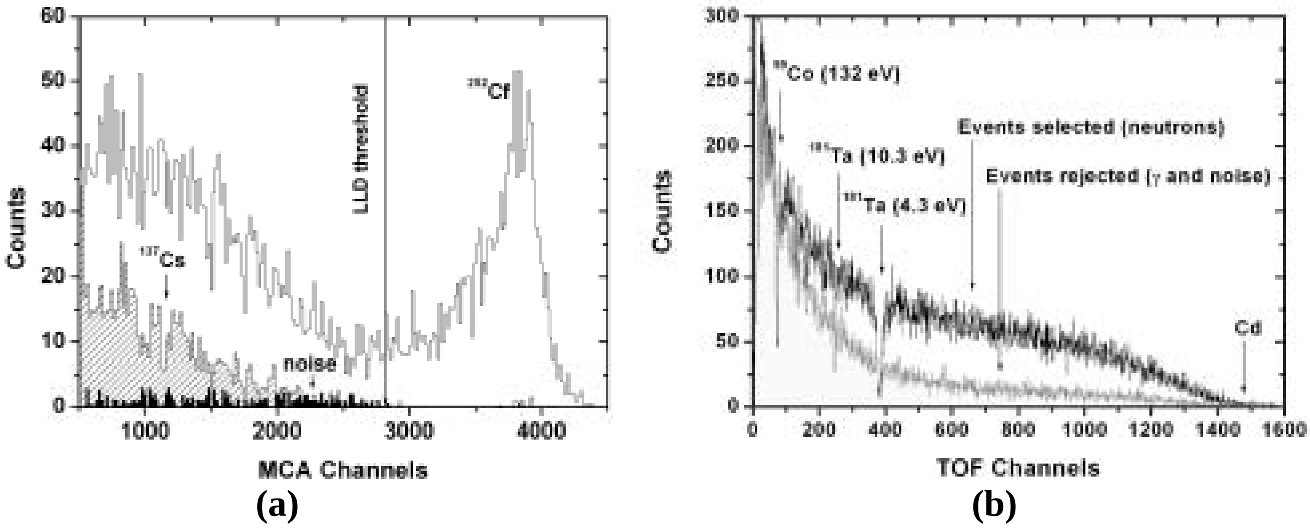

Fig. 3. (a) Pulse height spectra of γ rays from ^{137}Cs, neutrons and γ rays from ^{252}Cf, and noise from the neutron detector, (b) Neutron TOF spectra for events selected and rejected by the LLD setting value.

The effectiveness of this LLD value was tested with the neutron TOF spectra obtained by using notch-filters of Co, Ta and Cd, as shown in Fig. 3 (b). The upper solid curve was obtained with events selected by the LLD setting value, and the lower doted curve was obtained with events rejected by the LLD setting value. Figure 3 (b) demonstrates that the neutron-gamma separation circuit could discriminate gamma-rays from neutrons effectively.

We could estimate the background level by using resonance energies of the neutron TOF spectra of notch-filters of Co, In and Cd as shown in Fig. 4. The

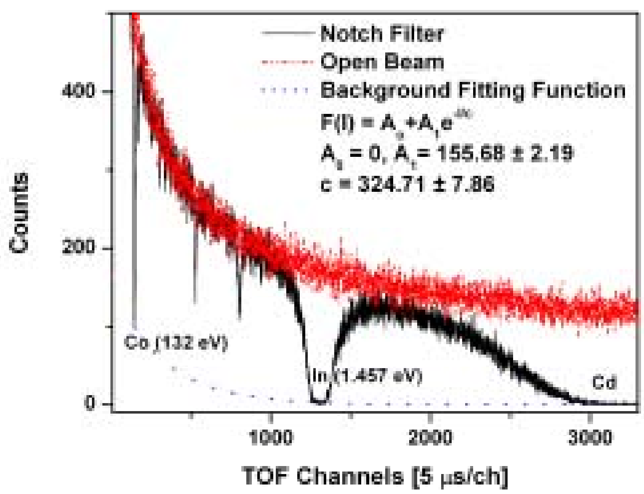

Fig. 4. Background level determination with Co, In, and Cd samples. The background fitting function was determined by using the black resonance energy of the notch filters.

magnitude of the background level was interpolated between the black resonances by using the fitting function $F(I) = A_0 + A_1 e^{-I/c}$, where A_0 , A_1, and c are constants and I is the channel number of the time digitizer.

The measurements were performed with two samples simultaneously. The two other positions of the sample changer were empty to collect the neutron TOF spectra without a sample (open beam). The positions of the samples were chosen in the following sequence: sample 1 – empty – sample 2 – empty. The exposition times for both sample 1 and sample 2 were 15 minutes (9000 pulses of PNF linac); for each empty position, it was 7.5 minutes. Thus, the durations for the samples were the same as those for the total open beam measurements. The interleaving sequence of free positions of the sample changer was chosen to minimize the influence of slow and/or/ small variation of the neutron beam intensity. If the beam intensity variations or its drift was fast and/or large, then these partial measurements were excluded from the total statistics. The total data taking times for Ag, Dy, W, and Ti were 65, 16, 48, and 43 hours, respectively, with the same times for the open beams.

The net neutron TOF spectra for the sample-in and the open beam for W and Dy as for an example are shown in Fig. 5, together with the estimated background level which is indicated by dash line. The neutron energy E in eV corresponding to each channel I in the TOF spectrum is derived from the relation $E = \{72.3 \times L/(I - I_0) \times W\}^2$, where L is the neutron flight path in meters, W is the channel width in microseconds, and I_0 is the channel of TOF=0 when the neutron burst was produced. In this experiment, we found I_0 to be equal to 5 channels.

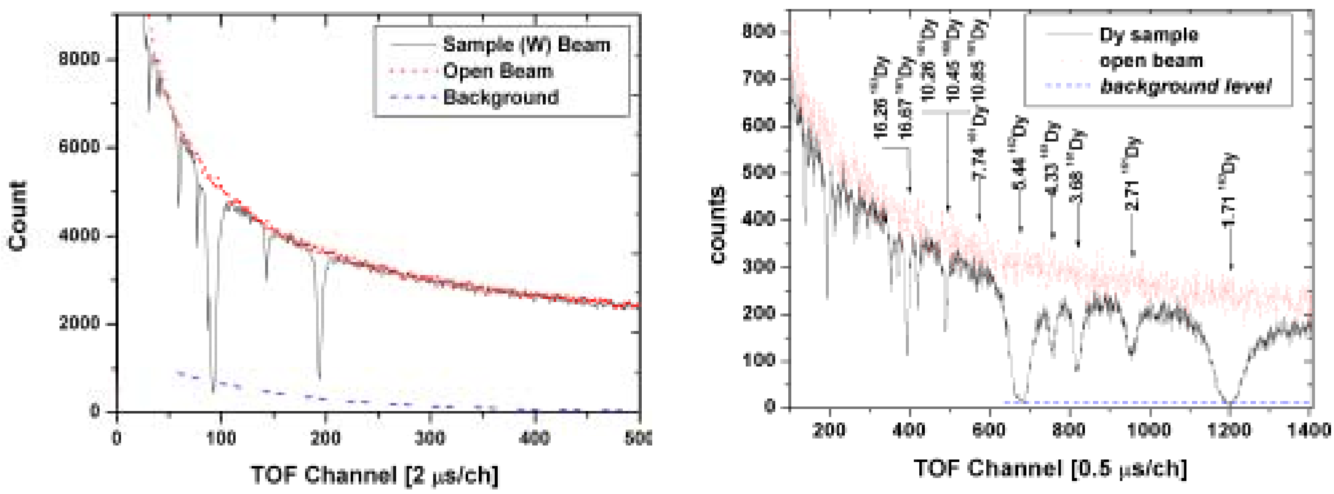

(a) **(b)**

Fig. 5. Neutron TOF spectra for the sample in and out for (a) W and (b) Dy samples, together with the background level indicated as a dotted line.

The neutron total cross-section is determined by measuring the transmission of neutrons through the sample. The transmission rate of neutrons at the i-th group energy E_i is defined as the fraction of incident neutrons passing through the sample compared to that in the open beam. Thus, the neutron total cross-section is related to the neutron transmission rate $T(E_i)$ as follows:

$$\sigma(E_i) = -\frac{1}{\sum_j N_j} \ln T(E_i) , \tag{1}$$

$$T(E_i) = \frac{[I(E_i) - IB(E_i)]/M_I}{[O(E_i) - OB(E_i)]/M_O} , \tag{2}$$

where N_j is the atomic density per cm^2 of the j-th isotope in the sample. $I(E_i)$ and $O(E_i)$ are the foreground counts for the sample in and out, $IB(E_i)$ and $OB(E_i)$ are the background counts for sample in and out, and M_I and M_O are monitor counts for the sample-in and the open beam, respectively. In this measurement, we assumed the monitor counts to be equal during the measurement.

IV. RESULTS AND DISCUSSION

The total cross-sections of natural W, Ti, Dy, and Ag were obtained in the energy range from 0.1 eV to 100 eV by using the neutron TOF method as shown in Fig. 6. We only considered the statistical errors for the present measurements because the other sources of uncertainties, which include the detection efficiencies, the geometric factor for the sample, and the other systematic errors, are negligible.

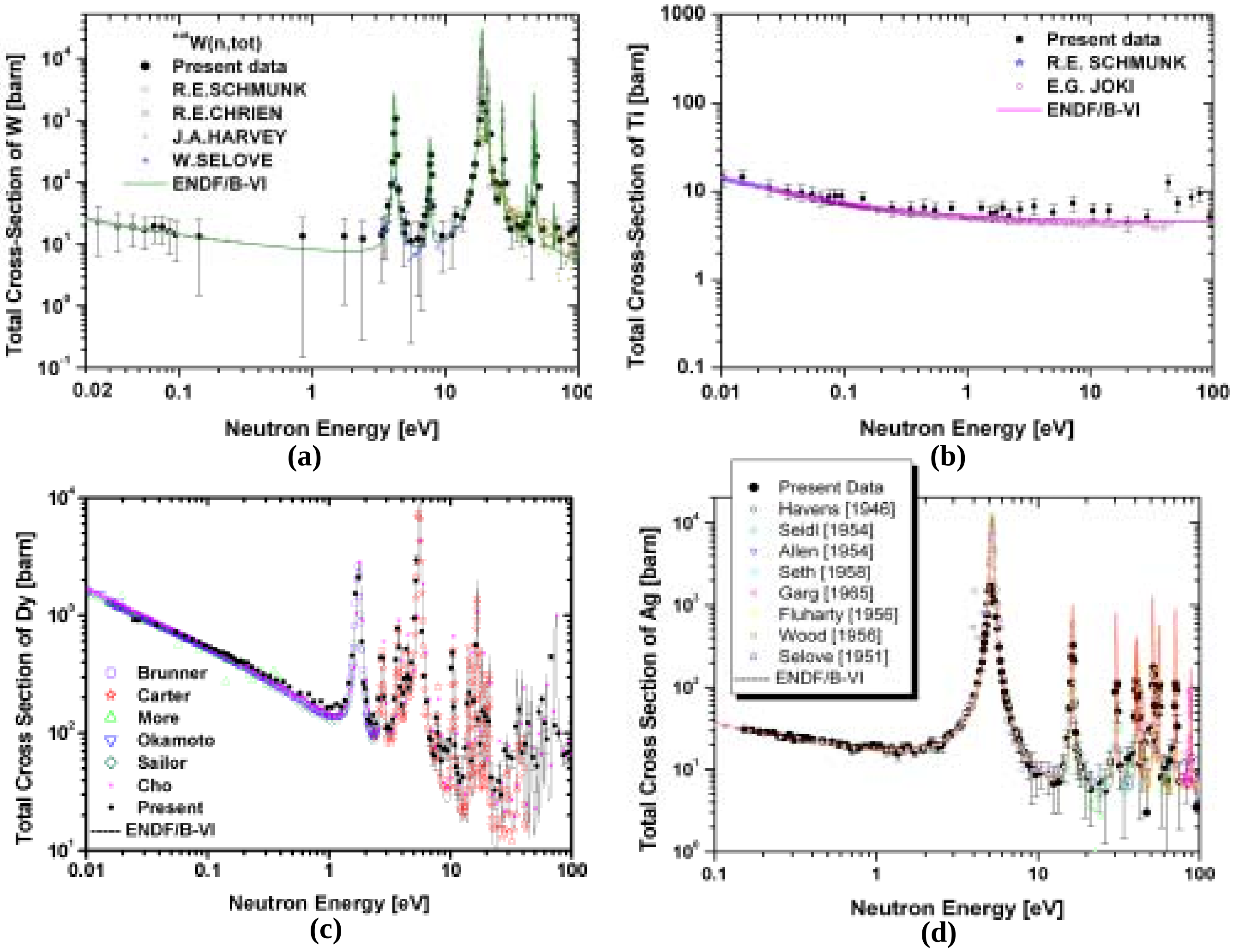

Fig. 6. Measured total cross sections for (a) W, (b) Ti, (c) Dy, and (d) Ag samples, respectively.

The present measurement for the neutron total cross-sections of natural W is compared with other data measured by Schmunk *et al.* [7], Chrien and Zimmerman [8], Harvey *et al.*[9], and Selove [10] and with the evaluated data in ENDF/B-VI [11] as shown in Fig. 6 (a). Figure 6 (b) shows the neutron total cross-sections for natural Ti compared with the other data measured by Schmunk *et al.* [7] and Joki [12] and with the evaluated data in ENDF/B-VI [11]. The neutron total cross-sections of Dy as shown in Fig. 6 (c) is compared with other data measured by Moore [13], Okamoto [14], Sailor *et al.* [15], Brunner et al. [16], Knorr et al. [17], Carter [18], and Cho et al. [19] and the evaluated data in ENDF/B-VI [11]. The present measurements for the neutron total cross sections of Ag is compared with other data measured by other groups [20] and the evaluated data in ENDF/B-VI [11] as shown in Fig. 6 (d). The present measurements without any corrections are generally in good agreement with other data and the evaluated one in the energy range between 0.1 eV and 100 eV.

There are many resonance peaks in the neutron total cross sections for Dy and Ag. In order to get the resonance parameters of each resonance peak, we fit the transmission data with the SAMMY code [21]. This code uses the Reich-Moore approximation [22] in the application of the R-matrix formalism. An implementation of Bayes' theorem is used to fit the requested resonance parameters to the data. For the Doppler broadening and resolution analysis, the MULTI method [23] is applied: the free gas model is applied to the Doppler broadening and the convolution of Gaussian and exponential function to the resolution. Resolution function $R(E,E')$ used in this calculation is the convolution of Gaussian and exponential function and its mathematical expression is as follows:

$$R_{GE}(E,E') = \frac{1}{\Delta_E \Delta_G \sqrt{\pi}} \int_{E-\Delta E_S}^{\infty} dE^0 \exp\left\{ -\frac{\left(E^0 - (E - \Delta E_S)\right)}{\Delta_E} \right\} \exp\left\{ -\frac{\left(E' - E^0\right)^2}{\Delta_G^2} \right\}, \tag{3}$$

where the width of Gaussian resolution function Δ_G is given by

$$\Delta_G = E[aE + b]^{1/2}, \tag{4}$$

and the width of exponential resolution function Δ_E is given by

$$\Delta_E = cE^{3/2}. \tag{5}$$

The energy shift ΔE_S, which is automatically determined in the SAMMY, is introduced in order to locate the maximum of the broadening function at $E' = E$. The constant values of a, b, and c are 1.3645×10^{-6} eV^{-1}, 9.1281×10^{-6}, and 6.3969×10^{-4} eV$^{-1/2}$, respectively.

The resonance parameters for the Dy and Ag isotopes have been obtained from the SAMMY fitting and listed in listed in Table 2 and 3, respectively, where they are compared with the existing data [24],[25] listed in the brackets. The quantity J and *l* is the spin of a particular resonance. The resonance energy of each state is generally in good agreement with the existing data.

Table 2. Resonance parameters for the Dy isotopes.

Dy Isotope	*J*	*E* (eV)		$g\Gamma_n$ (meV)	Γ_γ (meV)
163	2	Present	1.7093 ± 0.0007	0.9344 ± 0.0105	91.574 ± 0.827
		Mughabghab	(1.713 ± 0.004)	(0.85 ± 0.05)	(102.6 ± 0.8)
160	1/2	Present	1.8871 ± 0.0321	0.1394 ± 0.0135	124.97 ± 12.32
		Mughabghab	(1.88)	(0.20)	(105.80)
161	3	Present	2.6979 ± 0.0028	0.3929 ± 0.0122	130.12 ± 6.632
		Mughabghab	(2.71 ± 0.02)	(0.328 ± 0.015)	(119 ± 10)
161	2	Present	3.6618 ± 0.0025	0.9524 ± 0.0243	139.14 ± 6.087
		Mughabghab	(3.68 ± 0.03)	(0.89 ± 0.04)	(124 ± 15)
161	2	Present	4.2810 ± 0.0041	0.6677 ± 0.0273	130.25 ± 8.702
		Mughabghab	(4.33 ± 0.02)	(0.575 ± 0.065)	(80 ± 3)
162	1/2	Present	5.3697 ± 0.0022	14.492 ± 0.4007	262.08 ± 11.08
		Mughabghab	(5.44 ± 0.02)	(21 ± 1.5)	(148 ± 15)
163	2	Present	5.8377 ± 0.0775	0.0198 ± 0.0014	108.07 ±10.81
		Mughabghab	(5.81)	(0.0135)	(108.60)
161	3	Present	7.6632 ± 0.0195	0.4284 ± 0.0340	158.01 ± 14.46
		Mughabghab	(7.74)	(0.30)	(107.00)

Table 3. Resonance parameters for Ag isotopes.

Ag Isotope	J	l	E(eV)		Γ_γ (meV)	$g\Gamma_n$ (meV)
107	1	0	Present	-11.142	108.06	14.613
			Landolt-Boernstein	(-11.1)	(141.50)	(24.587)
107	0	0	Present	16.423±0.004	363.54±10.64	1.886±0.028
			Landolt-Boernstein	(16.3)	(134)	(2.917)
107	1	1	Present	18.899±0.140	100.00±10.00	0.000105±0.000011
			Landolt-Boernstein	(18.9)	(100)	(0.000105)
107	1	1	Present	20.323±0.147	99.99±10.00	0.00012±0.00001
			Landolt-Boernstein	(20.3)	(100)	(0.00012)
107	1	1	Present	35.826±0.233	99.997±10.00	0.000286±0.000029
			Landolt-Boernstein	(35.84)	(100)	(0.000285)
107	1	0	Present	41.726±0.0264	163.78±15.68	1.891±0.095
			Landolt-Boernstein	(41.57)	(137)	(4.5)
107	1	1	Present	42.751±0.276	100.00±10.00	0.003511±0.000351
			Landolt-Boernstein	(42.81)	(100)	(0.003495)
107	0	0	Present	45.264±0.118	150.12±14.94	0.462±0.0423
			Landolt-Boernstein	(44.9)	(147)	(0.3)
107	1	0	Present	51.756±0.018	314.97±24.32	7.286±0.219
			Landolt-Boernstein	(51.56)	(133)	(23.4)
107	1	1	Present	64.197±0.428	99.970±9.997	0.01951±0.001950
			Landolt-Boernstein	(64.24)	(100)	(0.018975)
107	2	1	Present	64.565±0.431	99.997±10.00	0.02631±0.000263
			Landolt-Boernstein	(64.74)	(100)	(0.0026)
107	1	1	Present	72.667±0.494	99.981±9.998	0.02722±0.00272
			Landolt-Boernstein	(73.21)	(100)	(0.027)
107	1	0	Present	82.827±0.598	139.07±13.91	0.01403±0.001403
			Landolt-Boernstein	(82.600)	(139.07)	(0.0014)
109	1	0	Present	5.186±0.001	(345.27±3.608)	4.4633±0.00032193
			Landolt-Boernstein	(5.145)	(143)	(9.6495)
109	1	0	Present	30.674±0.011	432.99±24.17	3.3719 ±0.0851
			Landolt-Boernstein	(30.6)	(130)	(6.33)
109	1	1	Present	32.694±0.214	100.09±10.01	0.0068938±0.000690
			Landolt-Boernstein	(32.7)	(100)	(0.0069975)
109	1	0	Present	40.492±0.020	231.62±19.89	2.7860±0.1113
			Landolt-Boernstein	(40.3)	(131)	(3.24)
109	0	0	Present	56.048±0.0318	171.55±16.32	4.8898±0.22453
			Landolt-Boernstein	(55.8)	(139)	(11.623)
109	1	0	Present	71.260±0.038	138.85±13.44	9.725±0.469
			Landolt-Boernstein	(71.)	(120)	(26.019)
109	1	0	Present	88.474±0.336	130.81±13.07	1.6569±0.15893
			Landolt-Boernstein	(87.7)	(130)	(4.70)

The measured total cross-section of Dy in the neutron energy range from 0.025 to 8 eV was compared with the SAMMY fitting results as shown in Fig. 7 (a). The SAMMY prediction of total cross-section and the present data are in good agreement with each other with $\chi^2/N=1.04$. In Fig. 7 (b), the measured total cross section of natural Ag in the neutron energy range from 1 eV to 65 eV was compared with the SAMMY fitting results. The SAMMY prediction of total cross section and the present data are in good agreement with each other with $\chi^2/N=1.41$.

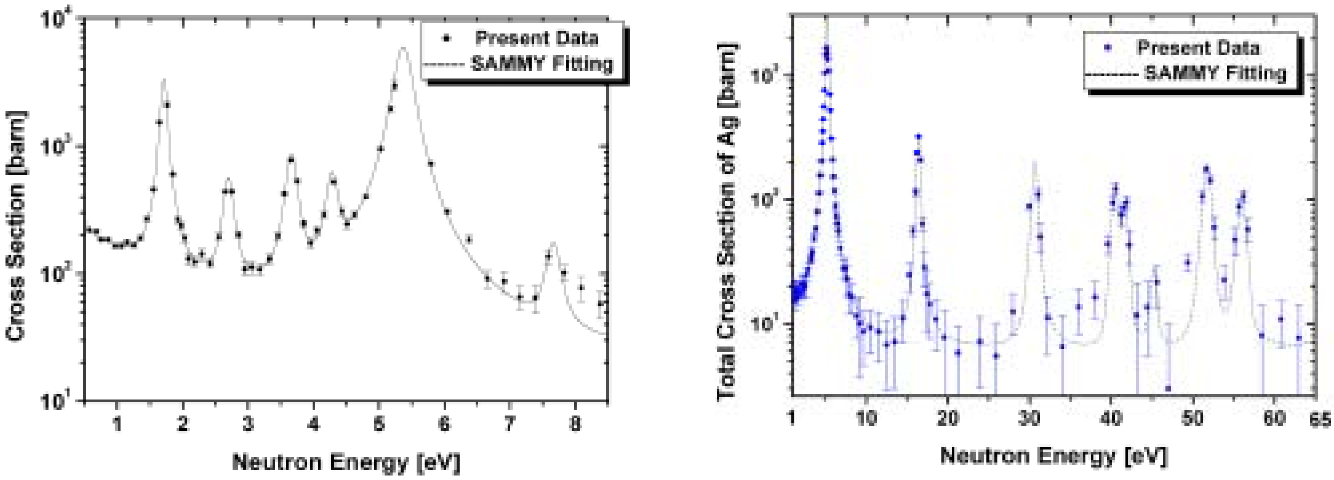

(a) (b)

Fig. 7. Comparison of the measured total cross sections of (a) Dy and (b) Ag with the predicted ones from the SAMMY fitting.

V. CONCLUSION

The Pohang Neutron Facility was constructed as a pulsed neutron facility based on an electron linac for producing nuclear data in Korea. It consists of an electron linac, a water cooled Ta target, and an 11-m long TOF path.

The neutron total cross-section of natural W, Ti, Dy and Ag have been measured in the neutron energy region from 0.025 eV to 100 eV by using a ^{6}Li-ZnS(Ag) scintillator and the neutron TOF method. The present results are in good agreement with the evaluated data in ENDF/B-VI and the previous measurements. The resonance parameters of Dy and Ag isotopes have been determined by fitting the transmission data and their results are also in agreement with the previous ones.

ACKNOWLEDGMENTS

The authors would like to express their sincere thanks to the staff of the Pohang Accelerator Laboratory for the excellent electron linac operation and their strong support. This work is partly supported through the Long-term Nuclear R&D program of the Korea Atomic Energy Research Institute and through the Science Research Center (SRC) program of the Institute of High Energy Physics, Kyungpook National University.

REFERENCES

[1] G. N. Kim, J. Y. Choi, M. H. Cho, I. S. Ko, W. Namkung, and J. H. Jang, in *Proceedings International Conference on Nuclear Data for Science and Technology*, edited by G. Reffo, A. Ventura and C. Grandi (Trieste, Italy, May 19-24, 1997), p. 556.

[2] H. S. Kang, J. Y. Choi, Y. J. Park, S. H. Kim, G. N. Kim, M. H. Cho, I. S. Ko, and W. Namkung, in *Proceedings of First Asian Particle Accelerator Conference*, edited by Y. H. Chin, M. Kihara, H. Kobayashi, N. Akasaka, K. Nigorikawa, and M. Tobiyama (Tsukuba, Japan, Mar. 23-27, 1998), p. 743.
[3] G. N. Kim, Y. S. Lee, V. Skoy, V. Kovalchuk, M. H. Cho, I. S. Ko, W. Namkung, D. W. Lee, H. D. Kim, S. K. Ko, S. H. Park, D. S. Kim, T. I. Ro, and Y. G. Min, J. Korean Phys. Soc. **38**, 14 (2001).
[4] W. Y. Baek, G. N. Kim, M. H. Cho, I. S. Ko, and W. Namkung, in Proceedings of Workshop on Nuclear Data Production and Evaluation, edited by J. Chang and G. N. Kim (Pohang, Korea, Aug. 7-8, 1998).
[5] G. N. Kim, V. Kovalchuk, Y. S. Lee, V. Skoy, M. H. Cho, I. S. Ko, W. Namkung, D. W. Lee, H. D. Kim, S. K. Ko, S. H. Park, D. S. Kim, T. I. Ro, and Y. G. Min, Nucl. Instr. Meth. **A 485**, 458 (2002).
[6] MCNP, A general Monte Carlo N-Particle transport code system, Version 4B, Los Alamos National Laboratory, LA-12625-M, (1997).
[7] R. E. Schmunk, P. D. Randolf, and R. M. Brugger, J. Nucl. Sci. Eng. **7**, 193 (1960).
[8] R. E. Chrien, and R. L. Zimmerman, Bull. Am. Phy. Soc., **3**, 19 (1958).
[9] J. A. Harvey, G. G. Slaughter, and R. C. Block, Bulletin of American Physical Society, **3**, 177 (1958).
[10] W. Selove, Phys. Rev. **84**, 864 (1951).
[11] R. F. Ross, ENDF-201, ENDF/B-VI Summary Documentation, BNL-NCS-17541, 4th Ed. (ENDF/B-VI), Brookhaven National Laboratory (1991).
[12] E. G. Joki, J. E. Evans, and R. R. Smith, J. Nucl. Sci. Eng. **11**, 298 (1961).
[13] W. M. Moor, Bulletin of American Physical Society, **6**, 70, (1961).
[14] K. Okamoto, JAERI Report, JAERI-1069 (1964).
[15] V. L. Sailor, H. H. Landon, and H. L. Jr. Foote, Phys. Rev. **96**, 1014 (1954).
[16] J. Brunner and F. Widder, Report EIR-123 (1967).
[17] K. Knorr and W. Schmatz, Atomk-ernenergie **16** (9), 49 (1970).
[18] R. S. Carter, Exfor Data File 11897 (1983).
[19] H. J. Cho, K. Kobayashi, S. Yamamoto, Y. Fujita, Y. S. Lee, G. N. Kim, I. S. Ko, M. H. Cho, W. Namkung, S. K. Ko, Annals of Nuclear Energy, **27**, 1259 (2000).
[20] W. W. Havens, Jr. and J. Rainwater, Phys. Rev. **70**, 154 (1946); W. Selove, Phys. Rev. **84**, 869 (1951); F. G. P. Seidi, D. J. Hugges, H. Palevsky, J. S. Levin, W. Y. Kato, and N. G. Sjostrand, Phys. Rev. **95**, 476 (1954); R. G. Allen, T. E. Stephenson, C. P. Stanford, and S. Bernstein, Phys. Rev. **96**, 1297 (1954); R. G. Fluharty, F. B. Simpson, and O. D. Simpson, Phys. Rev. **103**, 1778 (1956); R. E. Wood, Phys. Rev. **104**, 1425 (1956); K. K. Seth, D. J. Hughes, R. L. Zimmerman, and R. C. Garth, Phys. Rev. **110**, 692 (1958); J. B. Garg, J. Rainwater, and W. W. Havens, Jr., Phys. Rev. **137**, B547 (1965).
[21] N. M. Larson, RSICC Peripheral Shielding Routine Collection SAMMY-M2a: A Code System for Multilevel R-Matrix Fits to Neutron Data Using Bayes' Equations, PSR-158, SAMMY-M2a, Oak Ridge National Laboratory (1999) (unpublished).
[22] C. W. Reich and M. S. Moore, Phys. Rev. **111**, 929 (1958).
[23] F. A. George, "MULTI, A FORTRAN Code for Least-Square Shape Fitting of Neutron Cross-Section Data Using the Reich-Moore Multilevel Formalism," LA-5473-MS, Los Alamos Scientific Laboratory (1974).
[24] S. F. Mughabghab "Neutron Cross-sections," Vol.1, (Academic Press, NY, 1984).
[25] Landbolt-Boernstein/New Series: Numerical Data and Functional Relationships in Science and Technology, Group I: Elementary Particles, Nuclei and Atoms, Volume 16: Low Energy Neutron Physics, Subvolume B: Tables of Neutron Resonance Parameters, (Ed. by H. Schopper, Springer, Feb. 1998), pp. 197.